

Task-Specific Alignment and Multiple Level Transformer for Few-Shot Action Recognition

Fei Guo[†], Li Zhu^{*}, YiKang Wang[‡],

[†]School of Software Engineering, Xi'an Jiaotong University, Xi'an, China,
{co.fly, funnyQ}@stu.xjtu.edu.cn, lizhu@xjtu.edu.cn

Abstract—In the research field of few-shot learning, the main difference between image-based and video-based is the additional temporal dimension for videos. In recent years, many approaches for few-shot action recognition have followed the metric-based methods, especially, since some works use the Transformer to get the cross-attention feature of the videos or the enhanced prototype, and the results are competitive. However, they do not mine enough information from the Transformer because they only focus on the feature of a single level. In our paper, we have addressed this problem. We propose an end-to-end method named “Task-Specific Alignment and Multiple Level Transformer Network (TSA-MLT)”. In our model, the Multiple Level Transformer focuses on the multiple-level feature of the support video and query video. Especially before Multiple Level Transformer, we use task-specific TSA to filter unimportant or misleading frames as a pre-processing. Furthermore, we adopt a fusion loss using two kinds of distance, the first is L2 sequence distance, which focuses on temporal order alignment. The second one is Optimal transport distance, which focuses on measuring the gap between the appearance and semantics of the videos. Using a simple fusion network, we fuse the two distances element-wise, then use the cross-entropy loss as our fusion loss. Extensive experiments show our method achieves state-of-the-art results on the HMDB51 and UCF101 datasets and a competitive result on the benchmark of Kinetics and something-2-something V2 datasets. Our code will be available at the URL: <https://github.com/cofly2014/tsa-mlt.git>.

Index Terms—Few-shot action recognition, Task-Specific alignment, Multiple level Transformer, Optimal transport distance, Fusion network.

I. INTRODUCTION

VIDEO action recognition is an important research area. The rapid development of video action recognition based on deep learning is due to the use of a large amount of labeled videos [1]–[3]. However, the collection of video labels is time-consuming and labor-expensive. Consequently, the few-shot action recognition has received more and more attention due to the greatly reduced demand for labeled samples. For few-shot action recognition, earlier works tried to aggregate the representation of the support video in each class and get the prototype. The distribution of actions is not the same in different videos, not only the action speed is different, but also the key content occurs at different time points, and the action duration is often misaligned. In other words, the simple aggregation method ignores the important temporal

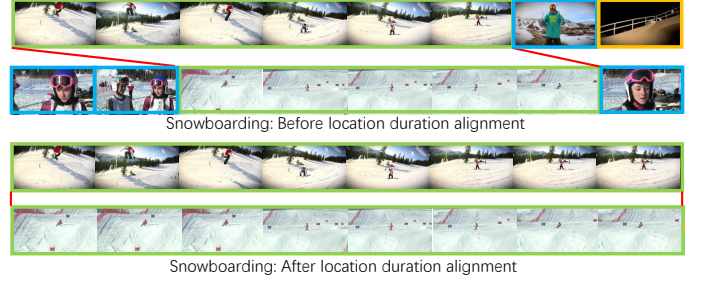


Fig. 1. The illustration shows the location-duration alignment. At the beginning and the end, there are a few frames that are less important or have misleading information. In the illustration, the frames with a blue border have less important information related to snowboarding, and the frame with a yellow border perhaps has misleading information related to snowboarding. Using the TSA, we aim to filter this information forcibly. For the action “snowboarding”, the upper is before the alignment, and the lower is after the alignment.

information of videos. Later, researchers introduced the attention mechanism and Transformer to address the spatial and temporal alignment, such as the TARN [4], ARN [5], TAEN [6], TRX [7], STRM [8]. Among these works, in 2021, TRX [7] selects a part-combination of tuples and gets the attention of certain tuples. For example, one Transformer branch extracts features from tuples that contain two frames, and another Transformer branch extracts features from tuples that contain three frames, it averages the class probability of the query sample from each Transformer branch and gets the final class probability. On one hand, for few-shot action recognition, the first step is frame sampling. Because the probability distribution of video action is various and the sampling operation is random, the action location-duration in frames is not the same, which is something that the above works ignore. In order to alleviate this problem, we need to filter out the less important or misleading information and get a better location-duration alignment (see Figure 1). On the other hand, for the TRX [7] related works, (1) they require different Cross-Transformer branches, which affects the flexibility of the model; (2) as the related works use all the tuples as features under certain cardinality, the computational cost will be large if the number of sampling frames increases, which may also cause overfitting; (3) these works ignore the relationship between representations of different levels (see in Figure 2). They only focus on the mapping of frame to frame or segment to segment.

In order to copy with the above problems, we devise a

^{*} BBB is the corresponding author.

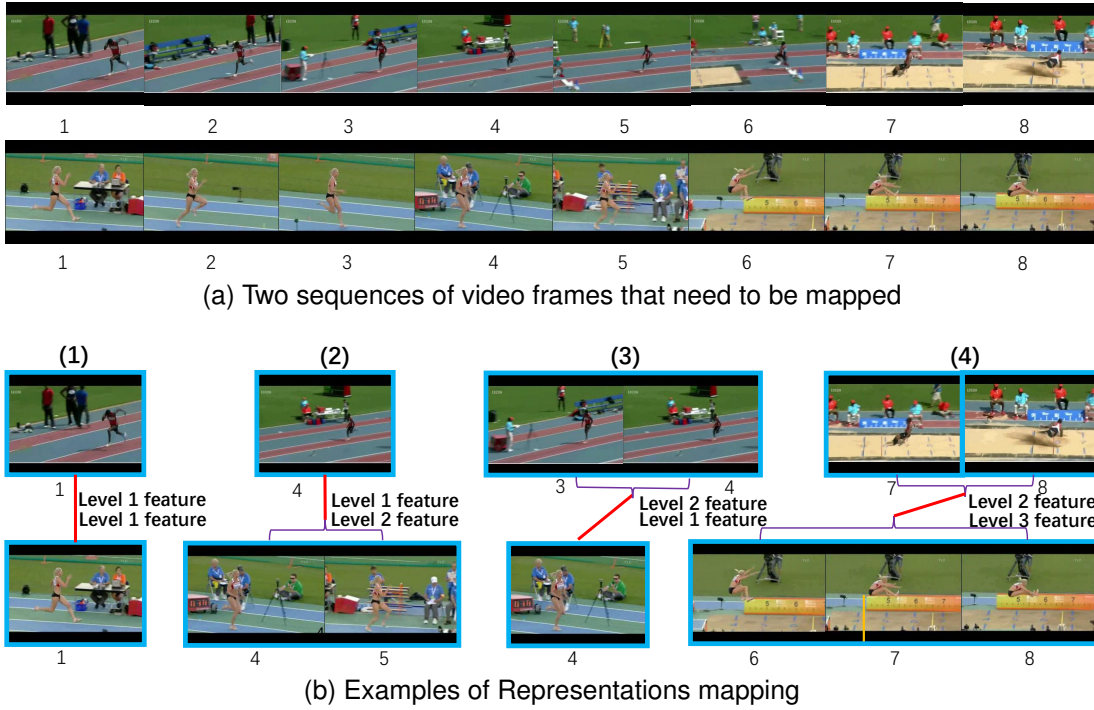


Fig. 2. Multiple level mapping. (a) It shows two sequences of video frames that need to be mapped. (b) (1) A single frame in the upper video can map a single frame in the lower video. (2) A single frame in the upper video can map the representation of level 2 in the lower video. (3) The representation of level 2 in the upper video can map a single frame in the lower video. (4) The representation of level 2 in the upper video can map the representation of level 3 in the lower video.

“Task-Specific Alignment and Multiple Level Transformer Network (TSA-MLT)” for few-shot action recognition. The first sub-module is **Task-Specific Alignment (TSA)**, the action location-duration of videos often has a misalignment issue, sometimes the first few or the last few frames are less important or misleading (see in Figure 1). Our TSA can adjust the location-duration from two directions. When the location-duration alignment network is well-trained, the filtering strategy is fixed, but in few-shot action recognition, tasks usually cause large inter-task variances, so using a fixed network to deal with the problem seems insufficient to always conduct good features. To this end, we adopt a task-adaptive learner, which generates Task-Specific parameters for the proportion of the output in two directions. The second sub-module is **Multiple Level Transformer (MLT)**, this sub-module aims to address the disadvantages of TRX [7], and STRM [8]. (1) Specifically, the Transformer we use focuses on multiple-level features. The multiple-level features contain tuples composed of different numbers of frames. Using the Transformer mechanism, a query-specific class prototype is constructed to match each multiple-level sequence of the query set. We suppose that the feature from different levels (contains different number of frames) can make the model more robust. Figure 2 shows some examples of how the multiple-level features match from the perspective of semantics. (2) Unlike the existing related works that need to create several Transformer instances based on the selection of cardinalities for the tuples, our MLT only requires one Transformer instance. (3) For each cardinality, we use a network to aggregate all the origin tuples into a small number of tuple representations.

In this way, we avoid a significant increase in computational cost as the number of sampling frames increases and also avoid overfitting. In addition to the aforementioned two sub-modules, we use both the sequence distance for mapping the tuples sequences, and the Optimal Transport distance which focuses on the appearance and semantics. Furthermore, we design a simple yet effective fusion network to combine the two distances.

Our contribution can be summarized as follows:

- (1) We propose a Task-Specific Alignment (TSA) module for filtering less important or misleading information in the first few or the last few frames in order to obtain an appropriate location-duration alignment. It is not only Task-Specific but also aligns from two directions.
- (2) We design a Multiple Level Transformer (MLT) module that uses multiple level features from different cardinalities to create the query-specific prototypes which are used to match the multiple-level features of query.
- (3) In our work, the Optimal Transport theory is introduced for the implementation of the appearance and semantic matching for the multiple-level features.
- (4) For the loss, we contact the distance of l_2 between two sequences and the distance of Optimal Transport element-wise, then use a network for a fusion distance which is used for the cross-entropy loss.
- (5) Extensive experiments have been conducted and the results on four benchmarks, HMDB51, UCF101, Kinetics, and Something-Something-V2, demonstrate that our TSA-MLT Network has a favorable performance and can compete with the state-of-the-art few-shot action

recognition methods.

II. RELATED WORK

A. Few-shot learning

The few-shot learning refers to the use of data samples that are far fewer than that required for deep learning to achieve close to or even exceed the effect of deep learning that uses large samples which are labeled. In recent years, as the investigation continues, researchers classify few-shot learning into three categories: (1) Metric-based methods [9]–[16] (2) Model-based methods [17]–[20] (3) Data-Augmentation based methods [21]–[25]. For example, Siamese Network [12] measures the similarity for a pair of images, Prototypical Network [10] computes the distances of Euclidean between the prototypes and queries, and MAML [17] is a meta-learning strategy that intends to learn a good model initialization of the parameters for a network that can rapidly adapt to new tasks. Multi-modal few-shot task [24] can generate extra images based on the text description to compensate for the lack of data.

B. Few-shot action recognition

Since 2018, many methods of few-shot action recognition have emerged. We can divide these works into the following categories: (1) Memory-based methods. CMN [26], and CMN-J [27] belong to this category, which encode the video representation using multi-significant embedding, and the key and value are stored in a memory and can be updated easily. “Few-shot action recognition with cross-modal memory network” [28] is also based on memory, and this work introduces the cross-modal: one modal is the video content, and another modal is the action label. SMFN [29] proposes to solve the few-shot video classification problem by learning a set of SlowFast networks enhanced by memory units. (2) Data-argument-based methods. ProtoGAN [30] uses a generative adversarial network with certain semantics as the condition to synthesize additional samples of novel classes for few-shot learning. AMeFu-Net [31] is also about data augmentation using depth features to enhance the information. (3) Metric-based methods for order matching. OTAM [32], computes the distance matrix following the DTW [33] method and makes a strict alignment. TARN [4] first introduced the attention mechanism for temporal alignment, its alignment is frame level. TRX [7] uses the Cross-Transformer to deal with frame tuples, then gets the tuples’ feature embedding alignment. The matching method of STRM [8] is similar to the TRX, and adds some pre-processing for feature enrichment. ARN [5] focuses on robust similarity, spatial and temporal modeling of short-term and long-term range action patterns via permutation-invariant pooling and attention. FAN [34] encodes videos and incorporates image features for comparison with an element-wise combination. (4) Metric-based methods for appearance and semantics. PAL [35] proposes a prototype-center loss and hybrid attention for order matching. CMOT [36] uses the Optimal Transport theory to compare the content of video not only focusing on the ordered alignment but also focusing on the video semantics. The HCR [37] uses a Wasserstein

distance to match the sequence of two sub-actions. “Few-Shot Learning of Video Action Recognition Only Based on Video content” [38] extracts the global video-level representation through aggregation.

Our work belongs to the category of metric-based methods for order matching, as well as involving metric-based methods for appearance and semantics.

III. METHODOLOGY

A. Problem Setting

In the field of few-shot action recognition, the video datasets are split into D_{train} , D_{test} , D_{val} , all the split datasets should be disjoint, which means there are no overlapping classes between each split dataset. In the D_{train} , it contains abundant labeled data for each action class, while there are only a few labeled samples in the D_{test} , and the D_{val} is used for model evaluation during the training episode. No matter D_{train} , D_{test} , or D_{val} , they all follow a standard episode rule. There are many episodes which are also called tasks during the training, testing, or validation. In each episode, N classes with K samples in D_{train} , D_{test} , or D_{val} are sampled as “support set”, the samples from the rest videos of each split DB are sampled as “query set”, just as P samples are selected from N classes to construct the “query set”. The goal of few-shot action recognition is training a model using D_{train} , which can be generalized well to the novel classes in the D_{test} only using $N \times K$ samples in the support set of D_{test} . Let $q = (q_1, q_2, \dots, q_m)$ represents a query video with m uniformly sampled frames. We use C to represent the set of classes, $C = \{c_1, \dots, c_n\}$, and the goal is to classify a query video q into one of the classes $c_i \in C$. In our work, the support set is defined as S , and the query set is defined as Q . For the class c , the support set S_c can be expressed as $S_c = \{S_c^1, \dots, S_c^k, \dots, S_c^K\}$, $1 \leq k \leq K$, and $S_c^k = (S_c^{k1}, \dots, S_c^{km})$, $1 \leq k \leq K$.

B. Overall framework

We propose a framework for few-shot action recognition as shown in Figure 3. Our work consists of five parts: (a) an Embedding Network Ψ_ϕ which extracts embedding features using the pre-training model on an enormous dataset; (b) a Task-Specific Alignment module (TSA) which is used for filtering out the less important or misleading information from two directions in order to get a location-duration alignment; (c) a Multiple Level Transformer module (MLT), it can aggregate different level information of certain video for a support video and query video, then the information of different levels are used to create the enhanced prototype with only one Transformer instance; (d) two types of distance: Sequence mapping distance which is order sensitive, Optimal Transport distance which is focused on minimizing the semantic gap between support and query; (e) a network for fusing the Sequence distance and Optimal Transport distance, the output of the network can obtain complementary information between two distances, and will be used for computing the cross-entropy loss.

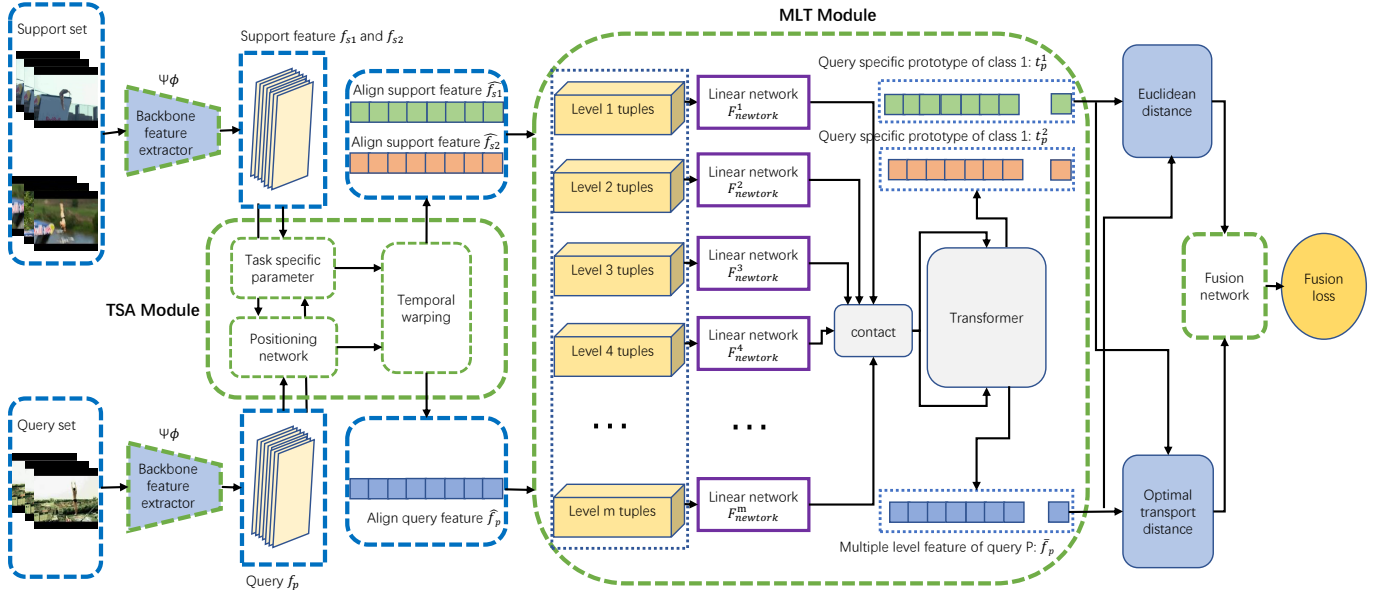


Fig. 3. The Framework of TSA-MLT. In this illustration, the visual workflow of our model can be seen as: (a) Backbone of RestNet50 (Ψ_ϕ). (b) Task-Specific Alignment (TSA). (c) Multiple Level Transformation (MLT). (d) Sequence order distance and OT distance compute. (e) Simple fusion network for the two distances. (Note: The green dashed areas represent the modules, while the blue dashed areas represent features in each step. For simplicity, we use a 2-way 1-shot setting in the illustration.)

C. Task-Specific Alignment module (TSA)

Linear sampling is used to align the action location-duration by filtering the frames that have less important information or have information that may mislead the video semantics at the beginning or the end of the video. We use the forward positioning network and backward positioning network to generate parameters for the Affine Transformation of the frames sequence in the time dimension. Because the probability distribution of videos in different tasks is often not the same, using a fixed network to generate the parameters of an Affine Transformation may lead to an inaccurate transformation. Therefore, we introduce a Task-Specific parameter network to generate the modulation parameters for the forward positioning network and backward positioning network according to the video samples in different tasks. As shown in Figure 4, the forward positioning network generates the affine parameter that will sample frames from the positive direction in the time axis, and the backward positioning network generates the affine parameter that will sample frames from the negative direction in the time axis. Meanwhile, modulation parameters in the positive and negative directions could be generated by Task-Specific parameter networks. Modulation parameters will assign the degree of sampling from the positive or negative direction. In TSA, our positioning network is designed based on 3D CNN, while our Task-Specific parameter network is designed based on 2D CNN. As in the formula (1) and formula (2), L_{fw} is the forward positioning network, and L_{bw} is the backward positioning network. f_X is the representation for both the support video and query video. In formula (3), T_{spec} is the network that will generate the modulation parameters for the positive and negative directions, and the F^s and F^q are the samples of support set and query set in each episode. And T_Δ is the Affine Transformation for the location shift

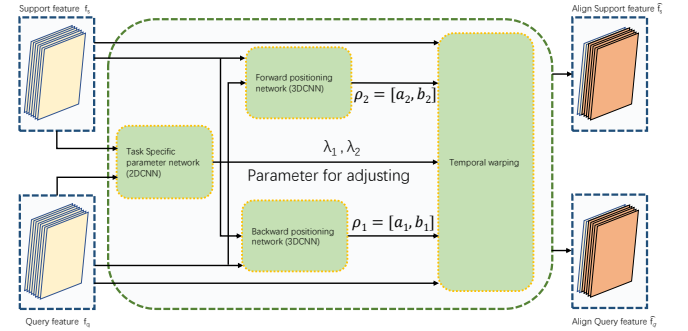


Fig. 4. The Task-Specific Alignment. Features are sent into the forward and backward positioning network, which will generate the parameters for warping. The Task-Specific parameter network will generate the modulation parameters that will assign the degree of two-direction warping.

with the affine parameter Δ just as formula (4).

$$\rho_1 = [a_1, b_1] = L_{fw}(f_X) \quad (1)$$

$$\rho_2 = [a_2, b_2] = L_{bw}(f_X) \quad (2)$$

$$\Theta = [\lambda_1, \lambda_2] = T_{spec}(F^s, F^q) \quad (3)$$

$$\hat{f} = T_\Delta(f_X), \quad \Delta = \Theta \cdot [\rho_1^T, \rho_2^T] \quad (4)$$

D. Multiple Level Transformer module (MLT)

Our MLT module gets inspiration from TRX-related works [7], [8], and aims to deal with the 3 problems motioned in section I. The detail is described as follows.

In Figure 3, following the rule of TSN [3], M frames are sampled from each video. For simplicity, we use a 2-way 1-shot setting as an example, f_{s1}, f_{s2} is support samples from the backbone, and f_p is the query sample from backbone,

the dimension of them is $C \times T \times H \times W$, where C is the number of channels, T is the number of frames, H and W are the dimension of 2D features. The $\hat{f}_{s1}, \hat{f}_{s2}, \hat{f}_p$ are the output of TSA, the dimension is the same as f_{s1}, f_{s2} and f_p . The number of tuples for different cardinalities should be " $C_M^1, C_M^2, \dots, C_M^M$ ". We use w to indicate the cardinality of the tuples. Just as $w = 1$ is for a single frame, which is for level one, $w = 2$ is for a pair which is level two, $w = 3$ is for a triple which is level three, \dots , $w = m$ is for the features of level m . We generalise to possible tuples for any w , just as formula (5):

$$\prod^w = (n_1, \dots, n_w) \in N^w : \forall i (1 \leq n_i < n_{i+1} \leq M) \quad (5)$$

where the M is the number of frames we sampled.

The associated query representation with respect to the tuple with indices $p = (p_1, \dots, p_w) \in \prod^w$, for the query tuple p , the query representation as formula (6):

$$Q_p^w = [\Phi(q_{p_1}) + PE(p_1), \dots, \Phi(q_{p_w}) + PE(p_w)] \in R^{w \times D} \quad (6)$$

where q_{p_1}, \dots, q_{p_w} are the representation of frames with the frame index as p_1, \dots, p_w . And $PE(\cdot)$ is a positional encoding given a frame index, and the Φ is a linear mapping which maps the dimension of each frame from $R^{H \times W \times H}$ to R^D .

For a tuple based on different cardinality w , the linear transformation as the formula (7) and formula (8):

$$\Upsilon^w, \Gamma^w : R^{w \times D} \rightarrow R^{d_k}, w \in \{1, \dots, m\} \quad (7)$$

$$\Lambda^w : R^{w \times D} \rightarrow R^{d_v}, w \in \{1, \dots, m\} \quad (8)$$

where $m \leq M$ is the largest cardinality we use.

In the TRX-related works, they have several Transformer instances according to how many cardinalities they use. If there are two cardinalities, as $\Omega = \{2, 3\}$, there should be two instances of Transformer, the first one has the linear translation of $\Upsilon^2, \Gamma^2, \Lambda^2$, and the second one has the linear translation of $\Upsilon^3, \Gamma^3, \Lambda^3$. In our work, there is only one Transformer instance named Multiple Level Transformer that averages the information of several frames in each tuple of each cardinality into one, then all the linear translations as formula (7) and (8) could be the same as $\Upsilon^1, \Gamma^1, \Lambda^1$. Through the improvement, we solve the problem for the flexibility of the model.

In our MLT, we define, when cardinality $w = 1$, the number of the tuples is N_1 , when $w = 2$, the number of the tuples is N_2 , ..., for $w = m$, the number of the tuples is N_m . For a sample, the feature dimension are $R^{N_1 \cdot d_k}$ for $w = 1$, $R^{N_2 \cdot d_k}$ for $w = 2$, \dots , $R^{N_m \cdot d_k}$ for $w = m$. All the features belong to different cardinalities w are contacted together, the contact operation ζ as formula (9) :

$$\zeta : R^{N_1 \times d_k}, R^{N_2 \times d_k}, \dots, R^{N_m \times d_k} \rightarrow R^{(N_1 + N_2 + \dots + N_m) \times d_k} \quad (9)$$

The more cardinalities we use, the more tuples there will be. If we use the cardinalities from $w = 1$ to $w = 8$, there will be 255 tuples. On one hand, a large number of tuples will take more memory. On the other hand, a large dimension of the feature will cause overfitting, and affect the accuracy of

model. So we generate a small number of tuple representations for certain cardinality with its total tuples. The formula (9) should be modified as formula (10):

$$\hat{\zeta} : R^{N_1 \times d_k}, R^{N_2 \times d_k}, \dots, R^{N_m \times d_k} \rightarrow R^{(\hat{N}_1 + \hat{N}_2 + \dots + \hat{N}_m) \times d_k} \quad (10)$$

we define a linear network under cardinality w as $F_{network}^w, w \in \{1, 2, \dots, m\}$, N_w is the input dimension which is equal to the total number of tuples under cardinality w , and \hat{N}_w is the output dimension which is equal to the number of tuple representations we will use. For each cardinality, we use a linear network to get a small number of tuple representations that can represent the whole tuples. In this way, we solve the problem that there are too many tuples under each cardinality as well as we can still benefit from the variety of whole tuples under each cardinality.

We define the set for a small number of tuple representations created using the linear network from $\prod^w, w \in \{1, \dots, m\}$ as $\overline{\prod}^w$, m is the largest cardinality we use. The correspondence between tuples of query P and S_{kt}^c which means tuple t of support video k in class c is calculated as the formula (11):

$$a_{k,t,p}^c = L(\Gamma^w \cdot S_{kt}^c) \cdot L(\hat{\zeta}(\Upsilon^1 \cdot Q_p^1, \Upsilon^2 \cdot Q_p^2, \dots, \Upsilon^m \cdot Q_p^m)), \\ t \in \overline{\prod}^w, w \in \{1, \dots, m\} \quad (11)$$

where L is a standard layer normalisation [39] and $Q_p^1, Q_p^2, \dots, Q_p^m$ is the feature of query P that based on the cardinality $1, 2, \dots, m$.

We apply the soft-max operation to acquire the attention map as the formula (12). Because the attention operation is executed after the linear operation Υ , and contact operation $\hat{\zeta}$. The across-attention matrix, for every item, includes not only the important measurement between single frames but also the important measurement for video semantics between different levels.

$$\hat{a}_{k,t,p}^c = \frac{\exp(a_{k,t,p}^c) / \sqrt{d_k}}{\sum_{l,n} \exp(a_{l,t,p}^c) / \sqrt{d_k}} \quad (12)$$

Then it is combined with value embedding of the support set as the following formula (13):

$$v_{kt}^c = \Lambda^w \cdot S_{kt}^c, w \in \{1, \dots, m\} \quad \text{and} \quad t \in \overline{\prod}^w \quad (13)$$

In order to compute the query-specific prototype with respect to the query P as the following formula (14):

$$t_p^c = \sum_{w=1}^m \sum_{k,t} \hat{a}_{kt,p}^c v_{kt}^c, t \in \overline{\prod}^w, w \in \{1, \dots, m\} \quad (14)$$

Using Optimal Transport distance in the next subsection to compare the multiple-level feature could solve the problem that TRX-related works ignore the relationship between the representations of different levels.

E. Optimal Transport distance

The optimal Transport issue aims at finding optimal transportation with the lowest cost between two distributions. Assuming a and b are two distributions, $a \in R^m$ and $b \in R^n$,

we aim to find a matrix $P \in R^{m \times n}$, P_{ij} means the probability of transferring from $a[i]$ to $b[j]$. We use $U(r, c)$ to represent all the possible solution space:

$$U(r, c) = \{P \in R^{m \times n} | P1_m = r, P^T 1_n = c\} \quad (15)$$

Given a cot matrix $M \in R^{m \times n}$, and the transfer plan P , the total cost can be represented by $\langle P, C \rangle$. The Optimal Transport problem is to find the most optimal transfer plan from r to c , which can be expressed by the following formula(16):

$$d_M(r, c) = \min \sum_{P \in U(r, c)} P_{ij} M_{ij} \quad (16)$$

using the Sinkhorn Algorithm [40], the equation (16) can be optimized through iteration. The optimal result of $U(r, c)$ is P^* .

The video matching problem could be described as an Optimal Transport problem [36]. Using the Optimal Transport theory, we can force our model to pay attention to the semantics and appearance of the video. In our paper, we focus on discrete Optimal Transport to formulate the video matching problem. After the MLT, we get the multiple-level representations f^{mul} , including the single frame feature(level 1 feature) and other high-level features, the rank of level is the same as the number of frames in an origin tuple, as the formula (17):

$$f^{mul} = \{\underbrace{f_1^1, f_1^2, \dots, f_1^{l_1}}_{level_1}, \underbrace{f_2^1, f_2^2, \dots, f_2^{l_2}}_{level_2}, \dots, \underbrace{f_m^1, f_m^2, \dots, f_m^{l_m}}_{level_m}\}, (n_{loss} M)_{fusion} = -\frac{1}{||Q||} \sum_{(P, y^p) \in Q, C} Y_p \cdot \log(p(y = c | P)) \quad (17)$$

where $m \leq M$ is the largest cardinality we use, l_1 is the number of frames we sample, l_2 is the number of small tuple representations created by the linear network for level 2 tuples, and the l_m is the number of small tuples created by the linear network for level m tuples. After using of Transformer in the MLT module, according to multiple level feature of a query P which is represented as \bar{f}_p , we can get the multiple level prototype in support set for class c as t_p^c . We assume the probability of t_p^c and \bar{f}_p is a uniform distribution. Then we define an array named *level*, the index of *level* represents the feature rank, and the value of each item in this array represents the number of tuple representations created by a linear network. The cost matrix C could be defined by the Euclidean distance (also other distances can be used here) between all the features at different levels as formula (18).

$$C = \langle \bar{f}_p, t_p^c \rangle, \quad C \in R^{(\sum_{i=1}^m \mathbb{I}(i)level[i]) \times (\sum_{j=1}^m \mathbb{I}(j)level[j])} \quad (18)$$

Note, we perhaps only use parts of the levels, not always the whole levels, so we use an indicator function \mathbb{I} to indicate whether we use the level.

In the end, the OT distance is defined as the formula (19):

$$distance_{ot}(\bar{f}_p, t_p^c) = CP^* \quad (19)$$

F. Sequence mapping distance

For the output of MLT, according to a certain query sample, we get the prototype of support set for class c as t_p^c , and

the representation of the query sample P as \bar{f}_p , the sequence mapping distance for each query video just as the formula (20):

$$distance_{seq}(\bar{f}_p, t_p^c) = ||\bar{f}_p, t_p^c||^2 \quad (20)$$

G. Loss for the fusion of OT Distance and Sequence mapping Distance

Given an N class problem, both the dimension of Optimal Transport distance and Sequence mapping distance should be N , we contact the distance element-wise as the formula (21):

$$distance_{contact} = contact(distance_{ot}, distance_{seq}) \quad (21)$$

where the dimension of $distance_{contact}$ is $2N$.

Then we define a simple but useful fusion network as (1) A fully connected linear layer with the dimension of input is $2N$, and output is N . (2) After the linear mapping, we use a Leaky ReLU operation. (3) Then we add a Batch Normalization operation.

We define the $distance_{fusion}$ as the output of the fusion network. Probabilities over class $c \in \{1, 2, \dots, N\}$ that decide which class the query sample P belongs to and the cross-entropy loss can be calculated as formula (22) and (23):

$$p(y = c | P) = \frac{\exp(distance_{fusion}(\bar{f}_p, t_p^c))}{\sum_{\hat{c}=1}^N \exp(distance_{fusion}(\bar{f}_p, t_p^{\hat{c}}))} \quad (22)$$

$$loss_{fusion} = -\frac{1}{||Q||} \sum_{(P, y^p) \in Q, C} Y_p \cdot \log(p(y = c | P)) \quad (23)$$

where $Y_p \in \{0, 1\}$ indicates if $y^p = c$. Q and C represent the query set and its corresponding class label set.

IV. EXPERIMENTS

A. Datasets

We train and evaluate the model on four datasets commonly used in the field of few-shot action recognition, including UCF101 [41], HMDB51 [42], Kinetics400 [43] and SSV2 [44]. Because our work focuses on few-shot learning, we need to properly segment the dataset. For Ssv2 and Kinesics, we use the split method of CMN [26], CMN-J [27]. The split method randomly selects a mini-dataset containing 100 classes, including 64 classes for training, 12 classes for validation, and 24 classes for testing, of which each class contains 100 samples. For Ssv2, we also use the OTAM [32] split method, which is similar to the Ssv2-CMN split method, except it uses all samples inside the class. In the OTAM, it contains 77500/1926/2854 videos included for *train/val/test* respectively, as some videos can not be found now, so in our work, it contains 67013/1926/2854 videos for *train/val/test* respectively. The UCF101 contains 101 action classes, according to the split in ARN [5], we selected 70 classes for training, 10 classes for verification, and 21 classes for testing, it contains 9154/1421/2745 videos for *train/val/test* respectively. For the HMDB51, we also follow the split rule of ARN [5], 31 classes for training, 10 classes for verification, and 10 classes for testing, with 4280/1194/1292 videos for *train/val/test*.

B. Implementation Details

Following the TSN [3] and previous methods, we sparsely and uniformly sample several (*i.e.* $T = 8$) frames for each video, then we flip each frame horizontally and randomly crop the center region of 224×224 for the training data augmentation. For the backbone, we use ResNet-50 [45] which is pre-trained on ImageNet [46], we remove the final fully-connected layer, and get the raw frame-level feature which has 2048 dimensions. In the meta-training phase, for the Ssv2 dataset, we randomly sample the support set and training set, and give 100000 episodes, for the Kinetics we sample 6000 episodes, and for HMDB51 and UCF101, we also sample 6000 episodes. In the meta-testing phase, we sample 10000 episodes and get the average accuracy of each episode. We utilize the SGD optimizer with a learning rate of 0.001 and 0.0001, and we train our model on Nvidia 3090 GPU. During training we thus average gradients and back propagate once every 16 iterations. For testing, we use only the center crop to augment the video.

C. Comparison with previous works

We compare the performance of our TSA-MLT with state-of-the-art methods including MatchingNet(2016) [13], ProtoNet(2017) [10], CMN(2018) [26], TARN(2019) [4], OTAM(2020) [32], CMN-J(2020) [27], ARN(2020) [5], AMeFu-Net(2020) [31], SMNF(2020) [29], PAL(2021) [35], CMOT(2021) [36], MPRE(2022) [47], HyRSM(2022) [48], TA2N(2022) [49], TRX(2021) [7], STRM(2022) [8], MoLo [50]. Table I shows the comparison with various state-of-the-art methods on UCF101 and HMDB51. Table II shows the comparison on Kinetics and Ssv2. The standard 5-way 1-shot setting and 5-way 5-shot setting tasks are scheduled for the test.

In Table I, for TRX and STRM, in the HMDB51 and UCF101, we give our implementation results for the 1-shot setting marked as red, as there is no result for the 1-shot setting. Based on the HMDB51, for the 5-shot setting, the performance of TSA-MTL has been improved to a certain extent compared with previous methods, and the accuracy has reached 78.2%. For the 1-shot setting, TSA-MLT accuracy is 57.9%, 3.8% higher than STRM, and 2% higher than TRX. For UCF101, 5-shot setting, the accuracy of TSA-MTL is 97.1% which is 0.2% higher than STRM, and 1% higher than TRX. For the 1-shot setting, the accuracy of TSA-MLT is 80.6%. **For 5-shot setting based on HMDB51, and the 5-shot setting based on UCF101 we achieve the state-of-the-art result.**

In Table II, for TRX and STRM, in the Kinetics and Ssv2, we mark our implementation results as red, the results are a little lower than that published, which may be due to the machine environment or random seed. In Kinetics, for the 5-shot setting, the accuracy that published for TRX is 85.9%, our implementation is 85.1%, the accuracy published for STRM is 86.7%, our implementation is 85.9%. The accuracy of TSA-MLT is 87.1%, it is higher than our implementation for both TRX and STRM(2% and 1.2% improved), but only 1.2% higher than that published by TRX and 0.4% higher than

that published by STRM. For the 1-shot setting, TRX releases 63.6%, and our implementation is 63.4%. STRM does not release the result for the 1-shot setting, and our implementation is 65.3%. The testing result of the 1-shot setting for TSA-MLT is 66.8%. **For a 5-shot setting based on Kinetics, our TSA-MLT achieves the state-of-the-art result.**

In Ssv2-all, for the 5-shot setting, TRX publishes the accuracy as 64.6%, our implementation is 63%, STRM publishes the accuracy as 68.1%, our implementation is 64.8%, and for TSA-MLT, the accuracy is 65.1%. For the 1-shot setting, the result published by TRX is 42%. STRM also does not publish for a 1-shot setting while our implementation is 42.9%. The accuracy of TSA-MLT is 43.8%. Based on Ssv2-all our results for 1-shot and 5-shot settings are higher than both the TRX and STRM of our implementation and are close to the state-of-the-art. In SSV2-part, for the 5-shot setting, TRX publishes the result as 59.4%, our implementation of STRM is 58.6%, a little lower than TRX, and our TSA-MLT is 60.9%, 1.5% higher than TRX. For the 1-shot setting, TRX publishes the result of 36.0%, for STRM our implementation is 38.3%, and the accuracy of TSA-MLT is 37.0%, 1% higher than TRX, and 1.3% lower than STRM. **For 5-shot setting based on Ssv2-part, our TSA-MLT achieve the state-of-the-art result 60.9%.** The other results are also competitive.

D. Ablation Study

1) *Analysis of Model Components:* In this part, we design and conduct some comparative experiments on Kinetics and UCF101 to evaluate the effectiveness of each part we construct. Here we still use the 5-shot and 1-shot for the evaluation.

In Table III, the experiment demonstrates, we have 2 important sub-modules, and the *fusion_loss* is for final classification. Except for the ablation of sub-modules, we still want to verify the fusion of Optimal Transport Distance and Sequence mapping Distance is effective, so we define *sequence_loss* and *ot_loss* which are similar to the formula (22) and (23), the only difference is that *distance_{seq}* as formula (19) is used for *sequence_loss* and *distance_{ot}* as formula (20) is used for *ot_loss*. In the experiment, our ablation parts are TSA, MLT, *sequence_loss*, *ot_loss*, and *fusion_loss*.

Overall, as the accuracies in Table III, using TSA and MLT with the fusion loss, the maximum performance can be achieved. We can summarize the ablation experiment: (1) Only using the MLT, our model can get a better performance than TRX under our implementation. it can be refer in Table I and II. (2) Under 5-shot setting, using the *fusion_loss* which is computed by the *distance_{fusion}*, the accuracy is increased compared to both *distance_{ot}* and *distance_{seq}*, because the *distance_{ot}* just brings the supplementary for semantic information and *distance_{seq}* just brings the order mapping information, but the *distance_{fusion}* carries both. (3) Under 1-shot setting, when using the *ot_loss* which is computed by the *distance_{ot}*, the accuracy is higher than using *distance_{fusion}*, perhaps because when there is one support sample, the information is not enough for sequence mapping, and the semantic information contains the sequence

Table I. Comparison on UCF101 and HMDB51. Results of classification accuracy for 5-way 1-shot setting, and 5-way 5-shot setting experiments are shown. * means the item contains our implementation. The data with * means the state of the art. The data marked as red indicates the results of our implementation,

Method	Reference	Backbone	HMDB51		UCF101	
			1-shot	5-shot	1-shot	5-shot
Machting Net [13]	NeurIPS'2016	ResNet-50	-	-	-	-
ProtoNet [10]	NeurIPS'2017	ResNet-50	54.2	68.4	74.0	89.6
CMN [26]	ECCV'2018	ResNet-50	-	-	-	-
TARN [4]	BMVC'2019	C3D	-	-	-	-
ARN [5]	ECCV'2020	C3D	44.6	59.1	62.1	84.8
AMeFu-Net [31]	MM'2020	ResNet-50	60.2	75.5	85.1	95.5
SMNF [29]	MM'2020	ResNet-50	-	-	-	-
PAL [35]	ARXIV'2021	ResNet-50	60.9	75.8	85.3	95.2
OTAM [32]	CVPR'2020	ResNet-50	54.5	66.1	79.9	88.9
CMOT [36]	ARXIV'2021	C3D	64.6*	77.0	90.4*	95.7
HyRSM [48]	CVPR'2022	ResNet-50	60.3	76.0	83.9	94.7
TA2N [49]	AAAI'2022	ResNet-50	59.7	73.9	81.9	95.1
MPRE [47]	TCSVT'2022	ResNet-50	57.3	76.8	82.0	96.4
MoLo [50]	CVPR'2023	ResNet-50	60.8	77.4	86.0	95.5
*TRX [7]	CVPR'2021	ResNet-50	55.9	75.6	77.3	96.1
*STRM [8]	CVPR'2022	ResNet-50	54.1	77.3	79.2	96.9
Ours(TSA-MLT)		ResNet-50	57.9	78.2*	80.6	97.1*

Table II. Comparison on Kinetics and Ssv2 datasets, for the classification accuracy. Results of 5-way 1-shot, and 5-way 5-shot experiments are shown. The Ssv2-part follows the split from [26], and the Ssv2-all follows the split from [32]. * means the item contains our implementation. The data marked as red in the parenthesis indicates the results of our implementation, reported results shown outside the parenthesis. The data with * means the state of the art.

Method	Reference	Backbone	Kinetics		Ssv2-part		Ssv2-all	
			1-shot	5-shot	1-shot	5-shot	1-shot	5-shot
Machting Net [13]	NeurIPS'2016	ResNet-50	53.3	74.6	34.4	43.8	-	-
ProtoNet [10]	NeurIPS'2017	ResNet-50	64.5	77.9	33.6	43.0	-	-
CMN [26]	ECCV'2018	ResNet-50	60.5	78.9	36.2	48.8	-	-
ARN [5]	ECCV'2020	C3D	63.7	82.4	-	-	-	-
AMeFu-Net [31]	MM'2020	ResNet-50	74.1*	86.8	-	-	-	-
SMNF [29]	MM'2020	ResNet-50	63.7	83.1	-	-	-	-
PAL [35]	ARXIV'2021	ResNet-50	74.2*	87.1*	-	-	46.4	62.6
OTAM [32]	CVPR's2020	ResNet-50	73.0	85.8	-	-	42.8	52.3
CMOT [36]	ARXIV'2021	C3D	-	-	-	-	46.8	55.9
HyRSM [48]	CVPR'2022	ResNet-50	73.7	86.1	40.6*	56.1	54.3	69.0*
TA2N [49]	AAAI'2022	ResNet-50	73.0	85.8	-	-	47.6*	61.0
MPRE [47]	TCSVT'2022	ResNet-50	70.2	85.3	-	-	42.1	58.6
MoLo [50]	CVPR'2023	ResNet-50	74.0	85.6	42.7	56.4	56.6*	70.6
*TRX [7]	CVPR'2021	ResNet-50	63.6(63.4)	85.9(85.1)	36.0	59.4	42.0	64.6(63.0)
*STRM [8]	CVPR'2022	ResNet-50	65.3	86.7 (85.9)	38.3	58.6	42.9	68.1(64.8)
Ours(TSA-MLT)		ResNet-50	66.8	87.1*	37.0	60.9*	43.8	65.1

information. (4)The accuracy in most items with the TSA is higher than without it. It can approve the effect of the TSA, even though sometimes the gap is small. Perhaps the probability of the phenomenon that the first and last several frames of the video contain invalid or misleading information is not high but does exist.

2) *Compare with varying cardinalities*: In Table IV, with the use of $TSA+MLT+fusion_loss$. Several different combinations of the cardinalities are selected, and it shows the accuracy of Kinetics and HMDB51 under a 5-shot setting. There are several linear network as $F_{network}^w, w \in \{1, 2, \dots, m\}$, as the formula (10), N_w as the dimension of input is the number of all tuples under certain cardinality w and \hat{N}_w is equal to

the number of tuple representations we will use. We just use five cardinalities in our experiment, for cardinality $w = 1$ we define $\hat{N}_1 = 8$, for cardinality $w = 2$ we define $\hat{N}_2 = 4$, for cardinality $w = 3$ we define $\hat{N}_3 = 3$ for cardinality $w = 4$ we define $\hat{N}_4 = 2$, for cardinality $w = 5$ we define $\hat{N}_5 = 1$. Among all the combinations in the table, we find that the $w = \{1, 2, 3, 4\}$ with the number of tuple representations as $\{8, 4, 3, 2\}$ is the optimal choice. It is also the configuration for Table I, Table II and Table III. For TRX, the optimal choice is $w = \{2, 3\}$, and the number of tuples is $84(28 + 56)$, for STRM, the optimal choice is based on the $w = \{2\}$, and the number of tuples is 28. We can see, the total number of tuples for our model is 17 under the optimal choice, much less than

Table III. Ablation for the Analysis of Model Components. The experiment is for the module of TSA and MLT with three types of loss. The Ablation study is under the datasets of Kinetics and HMDB51.

method	module part		loss			Kinetics		HMDB51	
	MLT	TAS	sequence_loss	ot_loss	fusion_loss	1-shot	5-shot	1-shot	5-shot
(1)	✓	✗	✓	✗	✗	64.2	85.4	52.9	75.8
(2)	✓	✗	✗	✓	✗	70.5	85.5	59.7	77.0
(3)	✓	✗	✗	✗	✓	67.5	86.5	57.5	78.1
(4)	✓	✓	✓	✗	✗	66.7	86.0	57.3	76.9
(5)	✓	✓	✗	✓	✗	71.0	85.5	60.0	77.1
(6)	✓	✓	✗	✗	✓	66.8	86.9	57.9	78.3

Table IV. Compare the accuracy of TLA-MLT with varying cardinalities.

No.	Cardinalities	tuples number	Kinetics	HMDB51
(1)	$\Omega = \{1\}$	8	85.3	75.8
(2)	$\Omega = \{1,2,3\}$	8+4+3(15)	85.6	77.9
(3)	$\Omega = \{1,2,4\}$	8+4+2(14)	86.5	77.8
(4)	$\Omega = \{1,2,5\}$	8+4+1(13)	86.0	76.7
(5)	$\Omega = \{1,3,4\}$	8+3+2(13)	85.3	78.2
(6)	$\Omega = \{1,3,5\}$	8+3+1(12)	84.9	76.9
(7)	$\Omega = \{1,4,5\}$	8+2+1(11)	85.2	75.9
(8)	$\Omega = \{1,2,3,4\}$	8+4+3+2(17)	87.1	78.2
(9)	$\Omega = \{1,2,3,5\}$	8+4+3+1(16)	85.9	76.4
(10)	$\Omega = \{1,2,4,5\}$	8+4+2+1(15)	86.6	77.7
(11)	$\Omega = \{1,3,4,5\}$	8+3+2+1(14)	85.8	78.0
(12)	$\Omega = \{1,2,3,4,5\}$	8+4+3+2+1(18)	85.4	76.2

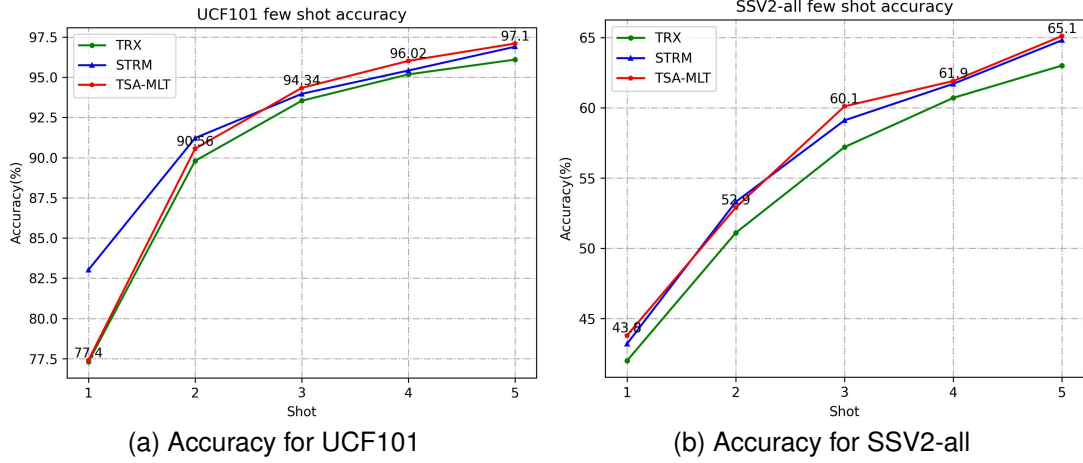


Fig. 5. The curve of the accuracies from 1-shot to 5-shot setting for the dataset of UCF101 and Ssv2-all.

the other methods.

3) *Performance of our model under the 5-way k-shot setting:* We test the performance of the model on Ssv2-all and UCF10. In Figure 5, the accuracy is for 1-shot to 5-shot of UCF101 and Ssv2-all. While the shots increase, the accuracy of each model also improves. It is worth noting that our method has consistently maintained leading performance compared to TRX and STRM models, except for UCF101 in 1-shot and 2-shot, the accuracy of our model is lower than others. It shows the robustness of our method. In Figure 5, the accuracies are following our own implementation.

V. VISUALIZATION

A. Accuracy comparison for different class

Compare with the TRX and STRM for the accuracy of the Kinetics. In our paper, we select 10 classes, and get the accuracy under the 5-shot setting, in Figure 6, it can be seen the accuracy of our model is improved for most of the classes from TRX and STRM except that the class “dancing charleston”. For the class “playing drums” the accuracy has the most improvement, from the accuracy of 90.82% of TRX and the accuracy of 89.83% of STRM to the accuracy of 95.17% of our model. The average accuracy for these 10 action classes

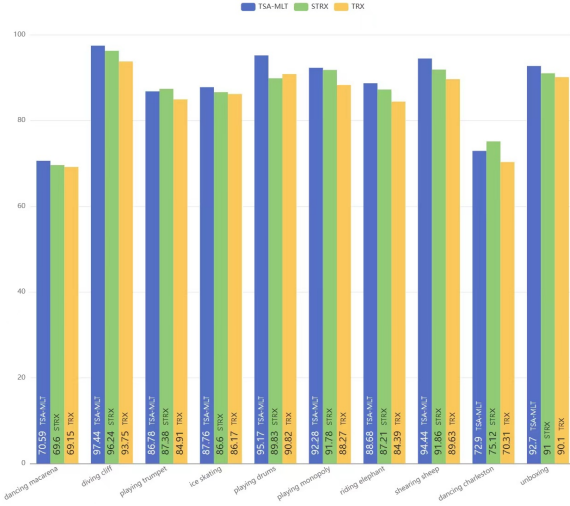


Fig. 6. The comparison of TRX, STRM, and TSA-MLT for the accuracy of certain action classes in the Kinetics dataset.

is improved from 84.75% of TRX and 86.66% of STRM to 87.87% of our TSA-MLT.

B. Distribution comparison

To prove that our model can get better feature distribution, we visualize the feature distribution of the prototype learned by TRX model, STRM model, and our TSA-MLT as shown in Figure 7 and 8 under 5-way 5-shot setting using t-SNE [51] on Kinetics and HMDB51. The illustrations show that the feature in different classes is more discriminative that the between-class scatter is larger, and the within-class scatter is smaller using TSA-MLT than other methods for both datasets.

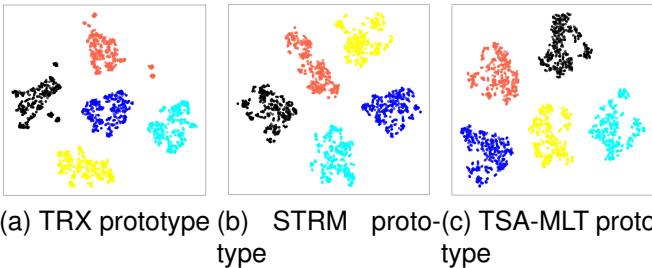


Fig. 7. The visualization of prototype feature distribution learned by (1) TRX vs.(2) STRM vs. (3) TSA-MLT on support samples for Kinetics under 5-way 5-shot settings. The visualization is performed with T-SNE.

C. Analysis of multiple feature attention score

In Figure 9, we can see the attention score map for Cross-Transformer with multiple level tuples. Each row represents the query features, and each column represents the support features. The area of “L1:L1” is the sub-attention score map for between level one representation, each row and column is the representation of a single frame in query features and support features, and the area of “L1:L2” is the sub-attention score map between level one representation in query features

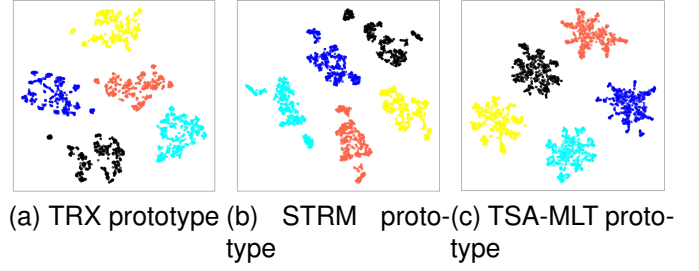


Fig. 8. The visualization of prototype feature distribution learned by (1) TRX vs.(2) STRM vs. (3) TSA-MLT on support samples for HMDB51 under 5-way 5-shot settings. The visualization is performed with T-SNE.

Attention score for Cross-Transformer with multiple level tuples representation

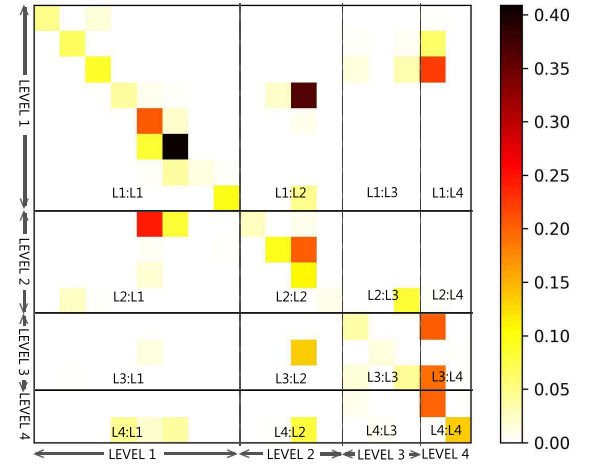


Fig. 9. The illustration shows the attention score map for Cross-Transformer with multiple level tuples.

and the level two representation in support features, each row is the representation of a single frame, and each column is the representation of the tuples that contain the information of 2 frames. Other areas also have a similar explanation. We can see there is a similarity between features not only at the same level but also at different levels. It makes sense that we use this multiple tuples attention map and the support features to compute the prototype in our paper, and each feature in the prototype contains information from different levels.

D. Analysis of Optimal Transport matrix P^*

In Figure 10, it is the optimal transfer plan matrix P^* , for example, the value in row i and column j is the probability of transferring distribution between i th query feature and the j th prototype feature. It can be seen that a diagonal has a large probability of transferring. The area of “L1:L1” shows the transfer probability between the level one representation of the query and the level one representation of the query prototype, the area of “L1:L2” shows the transfer probability between the level one representation of the query and the level two representation of the query prototype. And all the other areas show the transfer probability between same level or different

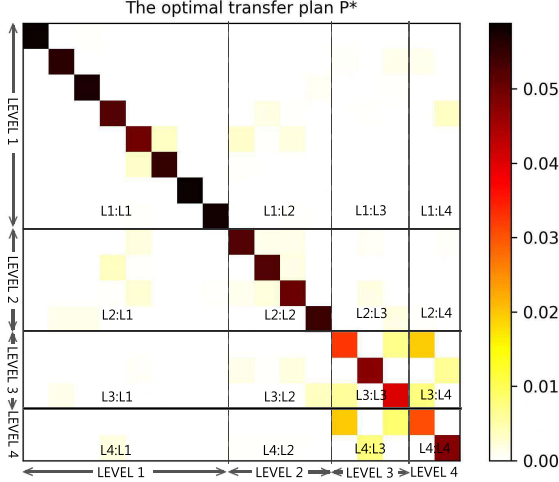


Fig. 10. The illustration shows an Optimal Transport matrix P^* of the Optimal Transport algorithm.

levels. The Figure 10 shows that features do have similarities not only from the same level but also from different levels.

VI. LIMITATION

Through experiments, it can be seen that our method has certain competitiveness in accuracy compared to other methods. However, under the meta-learning rule, for each episode, we may not have found the optimal cardinality combination and the number of selected tuples created by the simple networks under each cardinality, which can explore its maximum potential. There are too many combinations, So how to scientifically select these combinations and tuples is worth exploring in the future. In addition, for one-shot learning, the accuracy of our method is somewhat lower than the current SOTA, which may be due to the limitations of the method for selecting tuples under cardinality. How to solve this problem is also worth our further research. As the TSA module uses the 3DCNN and 2DCNN, it brings some computational complexity even though the MLT decreases the computational complexity. So how to simplify the TSA module is also worth studying.

VII. CONCLUSION

In this paper, we propose Task-Specific Alignment and Multiple Level Transformers for few-shot action recognition. Firstly, we design a TSA module that uses a 3DCNN to get the parameter for affine warping, and a CNN for task-specific adjustment, to filter some less important or semantically misleading frames. Secondly, we design a Multiple Level Transformer that gets several level semantic features of the video, from a single frame to the combinations of several frames. With this module, we can acquire different levels of semantic information about the video. Specifically, we use a simple linear network to decrease the number of tuples instead of using all the tuples under each level. Also, we design the

Optimal Transport distance for multiple-level features as a supplement to sequence distance. In the end, we use a fusion network to merge the two distances as a fusion distance. In the future, how to scientifically select these combinations and tuples is worth to be explored. In the end, we use a simple fusion network to fuse the Sequence distance and Optimal Transport distance, then acquire a fusion distance.

REFERENCES

- [1] Karen Simonyan and Andrew Zisserman. Two-stream convolutional networks for action recognition in videos. *Advances in neural information processing systems*, 27, 2014.
- [2] Du Tran, Lubomir Bourdev, Rob Fergus, Lorenzo Torresani, and Manohar Paluri. Learning spatiotemporal features with 3d convolutional networks. In *Proceedings of the IEEE international conference on computer vision*, pages 4489–4497, 2015.
- [3] Limin Wang, Yuanjun Xiong, Zhe Wang, Yu Qiao, Dahua Lin, Xiaoou Tang, and Luc Van Gool. Temporal segment networks: Towards good practices for deep action recognition. In *European conference on computer vision*, pages 20–36. Springer, 2016.
- [4] Mina Bishay, Georgios Zoumpourlis, and Ioannis Patras. Tarn: Temporal attentive relation network for few-shot and zero-shot action recognition. *arXiv preprint arXiv:1907.09021*, 2019.
- [5] Hongguang Zhang, Li Zhang, Xiaojuan Qi, Hongdong Li, Philip HS Torr, and Piotr Koniusz. Few-shot action recognition with permutation-invariant attention. In *Computer Vision–ECCV 2020: 16th European Conference, Glasgow, UK, August 23–28, 2020, Proceedings, Part V 16*, pages 525–542. Springer, 2020.
- [6] Rami Ben-Ari, Mor Shpigel Nacson, Ophir Azulai, Udi Barzelay, and Daniel Rotman. Taen: temporal aware embedding network for few-shot action recognition. In *Proceedings of the IEEE/CVF Conference on Computer Vision and Pattern Recognition*, pages 2786–2794, 2021.
- [7] Toby Perrett, Alessandro Masullo, Tilo Burghardt, Majid Mirmehdi, and Dima Damen. Temporal-relational crosstransformers for few-shot action recognition. In *Proceedings of the IEEE/CVF Conference on Computer Vision and Pattern Recognition*, pages 475–484, 2021.
- [8] Anirudh Thatipelli, Sanath Narayan, Salman Khan, Rao Muhammad Anwer, Fahad Shahbaz Khan, and Bernard Ghanem. Spatio-temporal relation modeling for few-shot action recognition. In *Proceedings of the IEEE/CVF Conference on Computer Vision and Pattern Recognition*, pages 19958–19967, 2022.
- [9] Christian Simon, Piotr Koniusz, Richard Nock, and Mehrtash Harandi. Adaptive subspaces for few-shot learning. In *Proceedings of the IEEE/CVF conference on computer vision and pattern recognition*, pages 4136–4145, 2020.
- [10] Jake Snell, Kevin Swersky, and Richard Zemel. Prototypical networks for few-shot learning. *Advances in neural information processing systems*, 30, 2017.
- [11] Flood Sung, Yongxin Yang, Li Zhang, Tao Xiang, Philip HS Torr, and Timothy M Hospedales. Learning to compare: Relation network for few-shot learning. In *Proceedings of the IEEE conference on computer vision and pattern recognition*, pages 1199–1208, 2018.
- [12] Iaroslav Melekhov, Juho Kannala, and Esa Rahtu. Siamese network features for image matching. In *2016 23rd international conference on pattern recognition (ICPR)*, pages 378–383. IEEE, 2016.
- [13] Oriol Vinyals, Charles Blundell, Timothy Lillicrap, Daan Wierstra, et al. Matching networks for one shot learning. *Advances in neural information processing systems*, 29, 2016.
- [14] Yanbin Liu, Juho Lee, Minseop Park, Saehoon Kim, Eunho Yang, Sung Ju Hwang, and Yi Yang. Learning to propagate labels: Transductive propagation network for few-shot learning. *arXiv preprint arXiv:1805.10002*, 2018.
- [15] Han-Jia Ye, Hexiang Hu, De-Chuan Zhan, and Fei Sha. Few-shot learning via embedding adaptation with set-to-set functions. In *Proceedings of the IEEE/CVF conference on computer vision and pattern recognition*, pages 8808–8817, 2020.
- [16] Wen Jiang, Kai Huang, Jie Geng, and Xinyang Deng. Multi-scale metric learning for few-shot learning. *IEEE Transactions on Circuits and Systems for Video Technology*, 31(3):1091–1102, 2021.
- [17] Chelsea Finn, Pieter Abbeel, and Sergey Levine. Model-agnostic meta-learning for fast adaptation of deep networks. In *International conference on machine learning*, pages 1126–1135. PMLR, 2017.

- [18] Andrei A Rusu, Dushyant Rao, Jakub Sygnowski, Oriol Vinyals, Razvan Pascanu, Simon Osindero, and Raia Hadsell. Meta-learning with latent embedding optimization. *arXiv preprint arXiv:1807.05960*, 2018.
- [19] Sachin Ravi and Hugo Larochelle. Optimization as a model for few-shot learning. In *International conference on learning representations*, 2017.
- [20] Yuanjie Shao, Wenxiao Wu, Xinge You, Changxin Gao, and Nong Sang. Improving the generalization of maml in few-shot classification via bi-level constraint. *IEEE Transactions on Circuits and Systems for Video Technology*, pages 1–1, 2022.
- [21] Alexander J Ratner, Henry Ehrenberg, Zeshan Hussain, Jared Dunnmon, and Christopher Ré. Learning to compose domain-specific transformations for data augmentation. *Advances in neural information processing systems*, 30, 2017.
- [22] Z Chen, Y Fu, Y Zhang, YG Jiang, X Xue, and L Sigal. Semantic feature augmentation in few-shot learning. *arxiv* 2018. *arXiv preprint arXiv:1804.05298*, 2018.
- [23] Luis Perez and Jason Wang. The effectiveness of data augmentation in image classification using deep learning. *arXiv preprint arXiv:1712.04621*, 2017.
- [24] Frederik Pahde, Mihai Puscas, Tassilo Klein, and Moin Nabi. Multi-modal prototypical networks for few-shot learning. In *Proceedings of the IEEE/CVF Winter Conference on Applications of Computer Vision*, pages 2644–2653, 2021.
- [25] Zhuohang Dang, Minnan Luo, Chengyou Jia, Caixia Yan, Xiaojun Chang, and Qinghua Zheng. Counterfactual generation framework for few-shot learning. *IEEE Transactions on Circuits and Systems for Video Technology*, pages 1–1, 2023.
- [26] Linchao Zhu and Yi Yang. Compound memory networks for few-shot video classification. In *Proceedings of the European Conference on Computer Vision (ECCV)*, pages 751–766, 2018.
- [27] Linchao Zhu and Yi Yang. Label independent memory for semi-supervised few-shot video classification. *IEEE Transactions on Pattern Analysis and Machine Intelligence*, 44(1):273–285, 2020.
- [28] Lingling Zhang, Xiaojun Chang, Jun Liu, Minnan Luo, Mahesh Prakash, and Alexander G Hauptmann. Few-shot activity recognition with cross-modal memory network. *Pattern Recognition*, 108:107348, 2020.
- [29] Mengshi Qi, Jie Qin, Xiantong Zhen, Di Huang, Yi Yang, and Jiebo Luo. Few-shot ensemble learning for video classification with slowfast memory networks. In *Proceedings of the 28th ACM International Conference on Multimedia*, pages 3007–3015, 2020.
- [30] Sai Kumar Dwivedi, Vikram Gupta, Rahul Mitra, Shuaib Ahmed, and Arjun Jain. Protogan: Towards few shot learning for action recognition. In *Proceedings of the IEEE/CVF International Conference on Computer Vision Workshops*, pages 0–0, 2019.
- [31] Yuqian Fu, Li Zhang, Junke Wang, Yanwei Fu, and Yu-Gang Jiang. Depth guided adaptive meta-fusion network for few-shot video recognition. In *Proceedings of the 28th ACM International Conference on Multimedia*, pages 1142–1151, 2020.
- [32] Kaidi Cao, Jingwei Ji, Zhangjie Cao, Chien-Yi Chang, and Juan Carlos Niebles. Few-shot video classification via temporal alignment. In *Proceedings of the IEEE/CVF Conference on Computer Vision and Pattern Recognition*, pages 10618–10627, 2020.
- [33] Meinard Müller. Dynamic time warping. *Information retrieval for music and motion*, pages 69–84, 2007.
- [34] Shaoqing Tan and Ruoyu Yang. Learning similarity: Feature-aligning network for few-shot action recognition. In *2019 International Joint Conference on Neural Networks (IJCNN)*, pages 1–7. IEEE, 2019.
- [35] Xiatian Zhu, Antoine Toisoul, Juan-Manuel Perez-Rua, Li Zhang, Brais Martinez, and Tao Xiang. Few-shot action recognition with prototype-centered attentive learning. *arXiv preprint arXiv:2101.08085*, 2021.
- [36] Su Lu, Han-Jia Ye, and De-Chuan Zhan. Few-shot action recognition with compromised metric via optimal transport. *arXiv preprint arXiv:2104.03737*, 2021.
- [37] Changzhen Li, Jie Zhang, Shuzhe Wu, Xin Jin, and Shiguang Shan. Hierarchical compositional representations for few-shot action recognition. *arXiv preprint arXiv:2208.09424*, 2022.
- [38] Yang Bo, Yangdi Lu, and Wenbo He. Few-shot learning of video action recognition only based on video contents. In *Proceedings of the IEEE/CVF Winter Conference on Applications of Computer Vision*, pages 595–604, 2020.
- [39] Jimmy Lei Ba, Jamie Ryan Kiros, and Geoffrey E Hinton. Layer normalization. *arXiv preprint arXiv:1607.06450*, 2016.
- [40] Marco Cuturi. Sinkhorn distances: Lightspeed computation of optimal transport. *Advances in neural information processing systems*, 26, 2013.
- [41] Khuram Soomro, Amir Roshan Zamir, and Mubarak Shah. Ucf101: A dataset of 101 human actions classes from videos in the wild. *arXiv preprint arXiv:1212.0402*, 2012.
- [42] Hildegard Kuehne, Hueihan Jhuang, Estíbaliz Garrote, Tomaso Poggio, and Thomas Serre. Hmdb: a large video database for human motion recognition. In *2011 International conference on computer vision*, pages 2556–2563. IEEE, 2011.
- [43] Joao Carreira and Andrew Zisserman. Quo vadis, action recognition? a new model and the kinetics dataset. In *proceedings of the IEEE Conference on Computer Vision and Pattern Recognition*, pages 6299–6308, 2017.
- [44] Raghav Goyal, Samira Ebrahimi Kahou, Vincent Michalski, Joanna Materzynska, Susanne Westphal, Heuna Kim, Valentin Haenel, Ingo Fruend, Peter Yianilos, Moritz Mueller-Freitag, et al. The” something something” video database for learning and evaluating visual common sense. In *Proceedings of the IEEE international conference on computer vision*, pages 5842–5850, 2017.
- [45] Kaiming He, Xiangyu Zhang, Shaoqing Ren, and Jian Sun. Deep residual learning for image recognition. In *Proceedings of the IEEE conference on computer vision and pattern recognition*, pages 770–778, 2016.
- [46] Jia Deng, Wei Dong, Richard Socher, Li-Jia Li, Kai Li, and Li Fei-Fei. Imagenet: A large-scale hierarchical image database. In *2009 IEEE conference on computer vision and pattern recognition*, pages 248–255. Ieee, 2009.
- [47] Shuwen Liu, Min Jiang, and Jun Kong. Multidimensional prototype refactor enhanced network for few-shot action recognition. *IEEE Transactions on Circuits and Systems for Video Technology*, 32(10):6955–6966, 2022.
- [48] Xiang Wang, Shiwei Zhang, Zhiwu Qing, Mingqian Tang, Zhengrong Zuo, Changxin Gao, Rong Jin, and Nong Sang. Hybrid relation guided set matching for few-shot action recognition. In *Proceedings of the IEEE/CVF Conference on Computer Vision and Pattern Recognition*, pages 19948–19957, 2022.
- [49] Shuyuan Li, Huabin Liu, Rui Qian, Yuxi Li, John See, Mengjuan Fei, Xiaoyuan Yu, and Weiyao Lin. Ta2n: Two-stage action alignment network for few-shot action recognition. In *Proceedings of the AAAI Conference on Artificial Intelligence*, volume 36, pages 1404–1411, 2022.
- [50] Xiang Wang, Shiwei Zhang, Zhiwu Qing, Changxin Gao, Yingya Zhang, Deli Zhao, and Nong Sang. Molo: Motion-augmented long-short contrastive learning for few-shot action recognition. *arXiv preprint arXiv:2304.00946*, 2023.
- [51] Laurens Van der Maaten and Geoffrey Hinton. Visualizing data using t-sne. *Journal of machine learning research*, 9(11), 2008.